radiation

MDPI

Article

Development of a Real-Time Radiation Exposure Estimation Method Using a Depth Camera for Radiation Protection Education

Toshioh Fujibuchi [1,*], Hiroyuki Arakawa [1] and Choirul Anam [2]

[1] Department of Health Sciences, Faculty of Medical Sciences, Kyushu University, 3-1-1 Maidashi, Higashi-ku, Fukuoka 812-8582, Japan; arakawa.hiroyuki.306@m.kyushu-u.ac.jp
[2] Department of Physics, Faculty of Sciences and Mathematics, Diponegoro University, Jl. Prof. Soedarto SH, Tembalang, Semarang 50275, Central Java, Indonesia; anam@fisika.fsm.undip.ac.id
* Correspondence: fujibuchi.toshioh.294@m.kyushu-u.ac.jp; Tel.: +81-92-642-6721

Simple Summary: X-ray fluoroscopy exposes physicians, radiation professionals, and patients to relatively high radiation. To reduce occupational exposure, understanding scattered radiation behavior is crucial. Our system estimates radiation exposure during fluoroscopy by monitoring the physician's position using a depth camera. We simulate the dose distribution of scattered radiation in an X-ray room using Monte Carlo code. Augmented reality markers display data, and body tracking estimates dose at joint points. The system's performance ranges from 9.0 to 11.0 FPS, with estimated doses 0.93 to 1.21 times the measured doses except for the chest and pelvis. Valuable insights into scattered radiation behavior are gained through joint point dose estimation.

Abstract: X-ray fluoroscopy causes relatively high radiation exposure to physicians, radiation professionals, and patients. Understanding the behavior of scattered radiation is crucial for reducing occupational exposure. We developed a system for estimating radiation exposure during fluoroscopy by monitoring the position of the physician using a depth camera for radiation protection education. The dose distribution of scattered radiation in an X-ray room was simulated using Monte Carlo code. The data were displayed using augmented reality markers, and the dose at each joint point location was estimated using body tracking. Additional functions were created, such as displaying arbitrary two-dimensional cross-sections. The system performance ranged from 9.0 to 11.0 FPS with or without motion and a protective apron. The estimated doses were 0.93 to 1.21 times the measured doses for all joint points, except for the chest and pelvis. The estimated doses for the chest and pelvis were lower than the measured dose, with the minimum values being 0.72 and 0.60 times lower for the chest and pelvis, respectively. The system provides valuable insight into the estimation of radiation dose at joint points based on the physician's position and movements, the physician's optimal fluoroscopy location, and warning of dangerous exposure doses.

Keywords: X-ray fluoroscopy; depth camera; body tracking; occupational exposure; Monte Carlo simulation

Citation: Fujibuchi, T.; Arakawa, H.; Anam, C. Development of a Real-Time Radiation Exposure Estimation Method Using a Depth Camera for Radiation Protection Education. *Radiation* **2024**, *4*, 261–275. https://doi.org/10.3390/radiation4030021

Academic Editor: Gabriele Multhoff

Received: 5 August 2024
Revised: 8 September 2024
Accepted: 12 September 2024
Published: 15 September 2024

1. Introduction

X-ray fluoroscopy and non-vascular interventional radiology (IVR) procedures, such as endoscopic retrograde cholangiopancreatography and percutaneous transhepatic biliary drainage, can result in significant radiation exposure, not only for patients but also for physicians and other healthcare personnel [1–3]. This heightened exposure is primarily due to the proximity of medical staff to both the X-ray tube and the patient, who serves as the primary source of scattered radiation in X-ray fluoroscopy rooms. This prolonged exposure to radiation poses risks of inducing cataracts in the eye lenses of medical staff [4,5].

Therefore, to promote radiation protection, the 2011 International Commission on Radiological Protection (ICRP) Seoul Statement recommended revising the threshold dose for cataracts and reducing the equivalent dose limit for lenses [6]. Proper training for radiation medical staff is essential to reduce radiation exposure to both patients and staff [7–9]. Understanding scattered radiation behavior is crucial in this educational process. However, comprehending radiation is challenging because of its invisible nature. Consequently, researchers are actively exploring ways of visualizing scattered radiation using technologies such as virtual reality (VR) and augmented reality (AR).

A previous study [10] depicted the distribution of scattered radiation corresponding to changes in the angle of the C-arm during angiography procedures using AR via tablets. While this study displayed radiation exposure on the surface of medical staff and patients using a color map, numerical values were not provided. Other prior research [7–13] has utilized virtual reality (VR) to visualize the spread of scattered radiation and its temporal changes in various examinations. However, the radiation dose variation due to changes in the position of medical staff within the X-ray room remains unknown. In another line of prior research [14], VR coupled with head-mounted displays was employed to immerse users in a virtual X-ray room, allowing for visualization of scattered radiation distribution at a scale corresponding to the environment. Conversely, one previous study [15] estimated the eye dose of operators within the virtual space. While there are numerous prior studies on AR and VR, there is currently no radiation protection education tool that visualizes scattered radiation in real space and estimates joint point doses in real time based on the position and movement of physicians.

To address this limitation, we employed AR technology to visualize an arbitrary two-dimensional cross-section of the scattered radiation distribution in real space, as captured by a camera. We expect that this approach will provide a more detailed depiction of the spread of scattered radiation and contribute to understanding the behavior of scattered radiation. Furthermore, to understand how much radiation exposure physicians receive based on their actions, we estimated the joint point radiation doses in real time using body tracking technology, corresponding to the real-time movements of physicians. This allowed us to comprehend hazardous high-dose areas. Physician exposure is high and uneven from point to point. To understand this practically, multiple dose estimates in real time are needed.

In this study, we developed a system for visualizing scattered radiation and estimating dose values at joint points in real time to enhance radiation protection education during X-ray fluoroscopy and non-vascular interventional radiology (IVR) with the over-couch X-ray tube-type unit. We evaluated the Monte Carlo simulation accuracy, joint point detection accuracy, real-time performance, and dose estimation accuracy of the developed system and examined its utility in radiation protection education.

2. Materials and Methods

2.1. System Creation

Azure Kinect (Microsoft, Redmond, WA, USA) is equipped with a time-of-flight (TOF)-type depth sensor. This camera can acquire red–green–blue color model (RGB) images, like a normal camera, as well as depth information and skeletal recognition. The game development platform Unity and the image-processing library OpenCV for Unity were used to develop the system. Depth and color images were acquired using Azure Kinect and imported into Unity on a PC equipped with a GPU. The distortion of the two cameras was calibrated using Azure Kinect's calibration function. ARmarkers were recognized, and body tracking was performed using OpenCV for Unity. The system components and an overview are shown in Figure 1, and the system development environment is presented in Table 1.

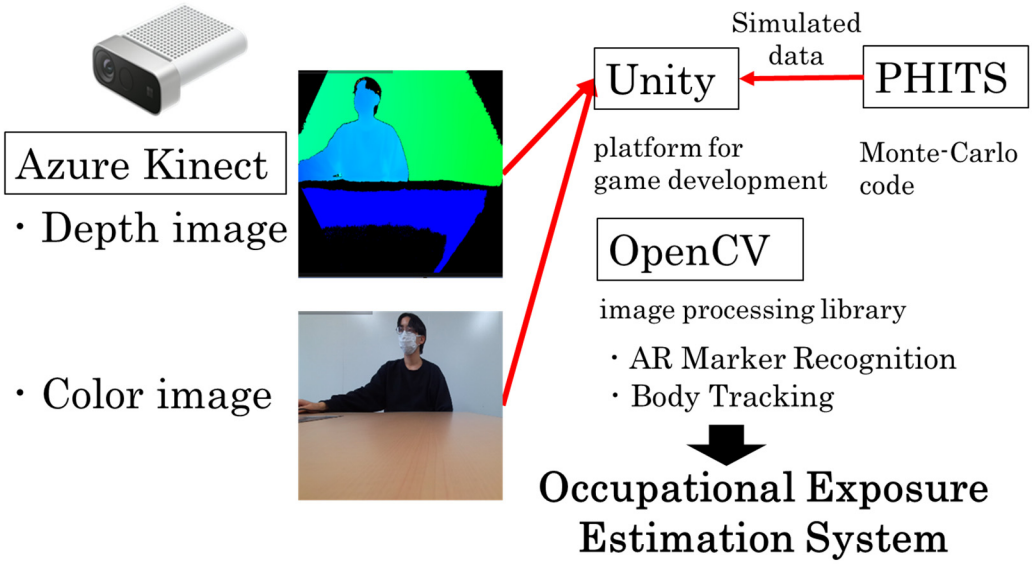

Figure 1. System components and overview. The AR marker information is captured using Azure Kinect's color image and superimposed in virtual space with the scattered ray distribution in the X-ray room calculated in advance using a Monte Carlo simulation. Furthermore, the body tracking of the physician is performed using Azure Kinect's depth image. These are integrated with Unity to estimate the radiation exposure of the physician in real time.

Table 1. Development environment of the system.

Specifications	Models
Operation system	Windows 10 64-bit Education 16 GB
Central processing unit	Intel Core i9-9980
Graphical processing unit	GeForce RTX 2080
Memory	32 GB
Depth camera	Microsoft Azure Kinect
Software	Unity 2020.3.8.f1 Azure Kinect Sensor SDK 1.4.1 Azure Kinect Body Tracking SDK 1.1.0 OpenCV for Unity 2.5.4

2.1.1. Calculation of Scattered Radiation Distribution in an X-ray Room

The behavior of scattered rays was simulated using the MC simulation code Particle and Heavy Ion Transport code system (PHITS) version 3.28 [16]. Photons were transported using the EGS5 (Electron-Gamma Shower version 5) code system in the PHITS setting [17]. EGS5 uses more recent photon cross-sections from the PHOTX library [18].

The irradiation conditions were a tube voltage of 87 kV with 2.5 mm Al filtration, a focus-to-image detector distance of 120 cm, and an irradiation field size of 15 × 15 cm^2. Various pieces of X-ray equipment, including an X-ray tube, an X-ray source, and a couch (height 80 cm from floor, length 235 cm, width 85 cm), were prepared in an X-ray room filled with an air of density 0.001293 g cm^{-3},with a composition of 80% nitrogen and 20% oxygen. The X-ray tube is an iron box with a density of 7.874 g cm^{-3} and a thickness of 5 mm, and the interior of the X-ray tube is vacuum. The collimator in the irradiation side of the X-ray tube is made of lead with a density of 11.34 g cm^{-3} and a thickness of 2 mm. The couch was made of carbon (density: 1.6 g cm^{-3}). In addition, an aluminum plate (density: 2.7 g cm^{-3}) that simulates a flat panel detector was placed behind the imaging site. The X-ray equipment was composed of iron. The subject was a 30 × 30 × 15 cm^3 water phantom.

An X-ray spectrum using Tucker's formula Version 4 (X-Tucker-4) [19], which is diagnostic region X-ray spectrum calculation software, was used to calculate the continuous

energy spectrum of a tube voltage of 87 kV and intrinsic filtration of 2.5 mm Al at 0.5 keV intervals. The obtained data were used as radiation sources. The number of histories in the MC simulation was set to 109. The cutoff energies were 10 keV for photons and 100 keV for electrons.

In the simulation, a cube of 5 cm on each side was constructed in a virtual X-ray room, the number of photons passing through the cube was counted, and the dose was detected using the fluence-personal dose equivalent factor of ICRP 74 [20]. The relative dose was calculated by dividing the fluence-personal dose equivalent factor by the entrance surface dose of 1 mGy per irradiation under the simulation conditions. The distance between the focal point and the incident phantom surface was 92.5 cm. The geometry of the simulation model is shown in Figure 2.

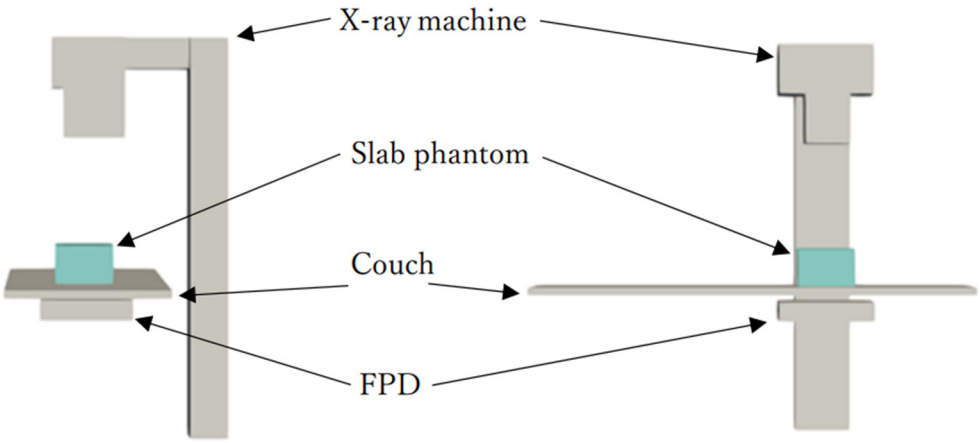

Figure 2. Model geometry. The X-ray device is an over-couch X-ray tube type, with a 20 cm thick water phantom placed above the bed to simulate the patient.

2.1.2. Body Tracking of the Physician in the X-ray Room

Body tracking was performed using Microsoft Azure Kinect, which recognizes 32 body parts and performs body tracking. The body tracking results were displayed on the game development platform Unity with reference to Microsoft's official sample [21] on GitHub, a source code management service for software development projects.

2.1.3. Display of Scattered Radiation Distribution with an AR Marker

The volume data of the X-ray machine, anthropomorphic phantom as a patient, and scattered radiation were displayed on Unity VR. An AR marker with dimensions of 24 cm (height) × 32 cm (width) was used to display these data, and the AR marker was placed above the X-ray tube to facilitate matching the focus of the actual X-ray tube with the focus of the simulated volume data. The coordinates were adjusted so that the two focuses coincided with respect to the lower left origin of the AR marker. The anthropomorphic phantom is an adult male form with a supine position placed on a couch.

2.1.4. Creation of Functions

Collision detection using the unity function was used to estimate the physician's exposure dose. The simulated volume data values at the positions of the body-tracked joint points were displayed. For the physician's dose estimation method, the X-ray examination room was divided into voxels at 5 cm intervals, and the individual dose equivalent rate Vp,r(x,y,z) [μSv/s] was registered in each voxel (coordinates x,y,z). By multiplying the dose equivalent rate of the physician's joint recognized by body tracking by the dose equivalent rate of the individual with the joint, the individual dose equivalent rate Hp,j,r(x,y,z) [μSv/s] at each joint was calculated by the following Equation (1).

$$H\text{p,j,r} = V\text{p,r(x,y,z)} \times \text{j(x,y,z)} \quad (1)$$

Here, by pressing the irradiate button during X-ray irradiation, the individual dose equivalent Hp,j,a [μSv] according to the pressed time t [s] was calculated by the following Formula (2).

$$H\text{p,j,a} = H\text{p,j,r} \times \text{t} \quad (2)$$

In addition, a function was created to display the dose distribution for an arbitrary two-dimensional cross-section. Functions to select the cross-section to display the dose distribution and to adjust the color scale were also created. A smoothing function was added to display the dose distribution.

2.2. Verification of the Accuracy of MC Simulation

The scattered radiation distribution data obtained by the simulation in PHITS were analyzed using ParaView visualization software. ParaView was used to obtain the dose at six locations in the X-ray room for the simulated data at heights of 100, 150, and 200 cm. The measured positions are shown in Figure 3. The relative doses obtained in the simulations were the personal dose equivalents normalized by the entrance surface dose of the water phantom. The relative doses were then obtained using RaySafe X2 (Unfors RaySafe AB, Billdal, Sweden) to measure the entrance surface dose. The dosimeter was compared and found to agree with the values of an ionization chamber dosimeter calibrated by a calibration laboratory. The specifications of the dosimeter adhere to the X-ray meter standard (IEC 61674), with a dose range of 1 nGy to 9999 Gy, a dose rate range of 1 μGy/s to 500 mGy/s, and a kV range of 40–130 kV. The sensor consists of a multilayered structure of semiconductors with varying filtration rates.

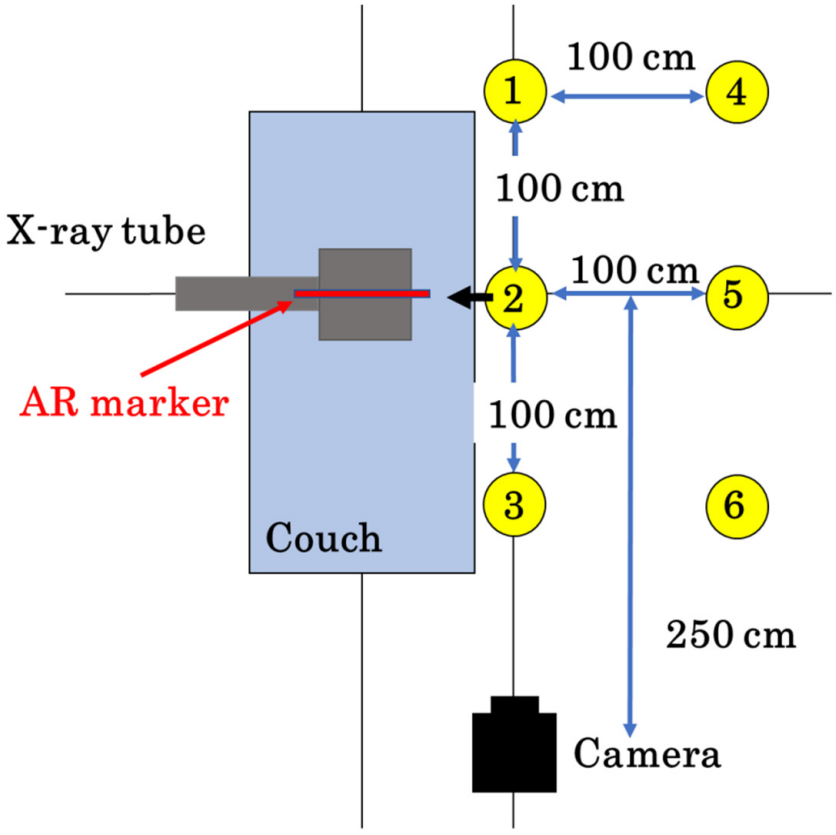

Figure 3. Equipment geometry and measurement positions. The upper field AR marker of the X-ray tube was fixed and placed. The Azure Kinect was placed at a height of 200 cm using a tripod. Numbers 1 to 6 are dose assessment points that assume the physician's position at 100 cm intervals. Tripods were set up here and dosimeters were placed.

RaySafe i3 (Unfors RaySafe AB, Billdal, Sweden) was used to measure the personal dose equivalent at the same locations in the X-ray room. The dosimeters were calibrated to the Personal Dose Equivalent Hp(10) by the manufacturer within one year. The accuracy of these dosimeters (angular dependence, energy dependence, stability, reproducibility, etc.) has been shown in previous study [22]. Raysafe i3 can efficiently measure personal dose equivalent at many points. Our purpose was to estimate the personal dose equivalent. Therefore, we used this dosimeter. Measurements were taken three times using dosimeters, and a comparative analysis was carried out between the simulated and measured values.

2.3. Verification of Position Detection Accuracy

A mannequin (SD206RE, Sun Create Co., Ltd., Oita, Japan) was used to verify the accuracy of physician body tracking. The height of the mannequin was 180 cm, and its surface color was an ivory tricot. The distance from the bottom-right of the AR marker to each joint point was acquired from the system and measured using a laser rangefinder. Subsequently, the distance acquired from the system was then compared to the actual distance measured. Measurements were taken at positions 1, 2, 3, and 5, as shown in Figure 3. The discrepancies in the simulations were addressed by fine-tuning the parameters of the X-ray tube structure that were unclear.

2.4. Verification of Real-Time Performance

To determine whether the system operated smoothly, the real-time performance of the system was evaluated by measuring the number of frames per second (FPS) through the Stats function. FPS measurements were conducted across four physician conditions as follows: with and without the physician moving at 25 cm/s, and with and without the protective apron. The protective apron (SLB-25M, MAEDA & Co., Ltd., Tokyo, Japan) provided only front protection and had an orange color (Figure 4). The resulting measurements were subjected to Welch's t-test using Excel 2021.

Figure 4. Body tracking a physician wearing a protective apron.

2.5. Verification of Dose Estimation Accuracy

A mannequin was used to verify the accuracy of dose estimation using the system. personal dose equivalents were measured by attaching RaySafe i3 at seven joint points (right eye, left eye, neck, chest, pelvis, right hand, and left hand) where the system could acquire the doses. The mannequins were measured at three locations (1, 2, and 3 in Figure 2). The doses were also obtained using the developed system and subsequently compared to the actual measurements. Dosimeters were attached to mannequins by tape. Dosimeter placement points on the mannequin were marked to improve reproducibility and reduce errors in dose estimation.

3. Results

3.1. System Overview

Figure 5 presents the actual usage interface of the developed system. On the left, simulation data depicting scattered radiation overlays the X-ray room's point-cloud data. This display enables the observation of the scattered radiation distribution within an arbitrary two-dimensional cross-section. Additionally, the interface allows for the selection of specific two-dimensional cross-sections of scattered radiation for display, providing adjustable color scaling. Moreover, a smoothing function was incorporated to enhance the visual presentation of the dose distribution. On the right side of the interface, the prominently featured dose estimation function displays the doses at each joint point, conveyed through both color and numerical values near each joint point. The dose values are the personal dose equivalents normalized by the entrance surface dose of the water phantom.

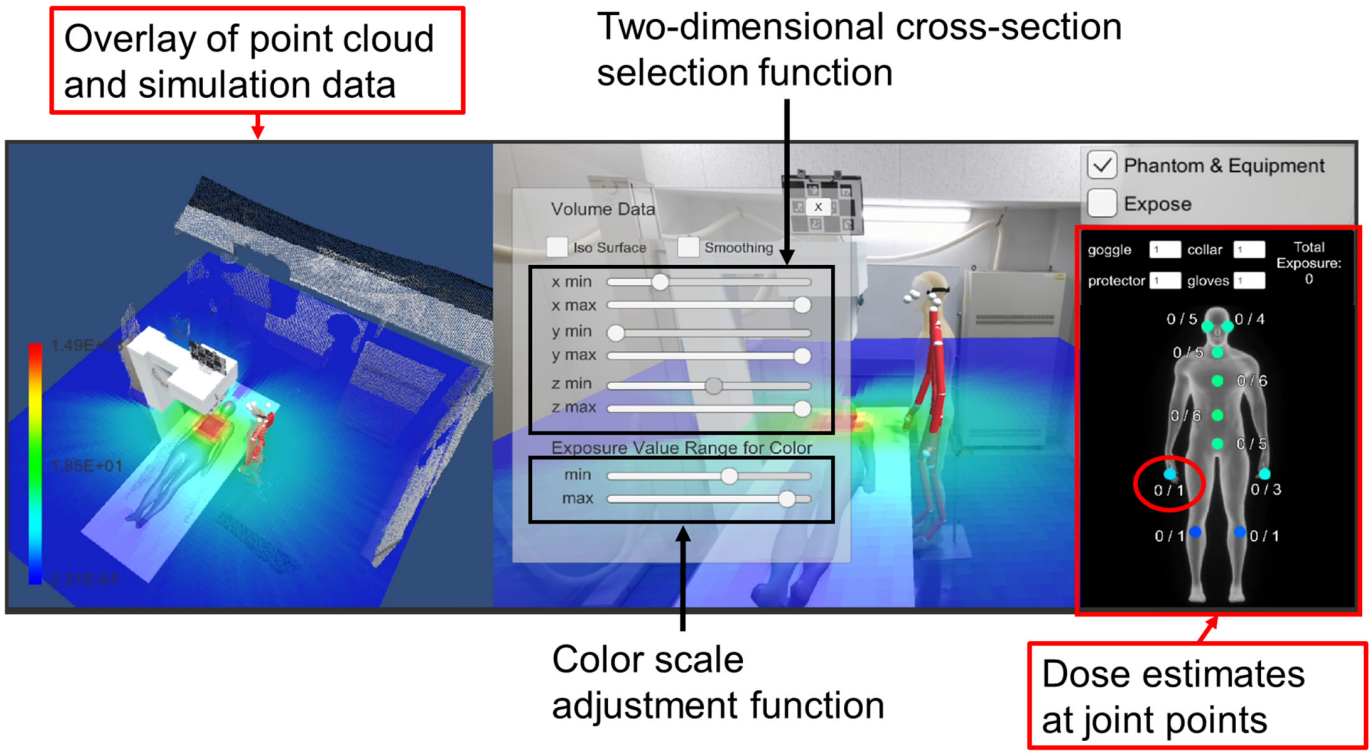

Figure 5. Screenshot of the developed system in use.

Figure 6 shows the X-ray room when this system is used. The 50-inch large display is placed close to the wall of the room; then, the physician can easily observe the interface.

Figure 6. Arrangement of equipment in the X-ray room when using the system.

3.2. Validation of MC Simulation Accuracy

Figure 7 illustrates the ratios between the simulated and measured personal dose-equivalent values at six distinct locations and three different heights within the X-ray room. The error bars indicate standard deviations resulting from variations in dosimeter measurements. The ratio of measured to estimated values ranges from 80% to 120%. Ideally, this ratio should remain at 100% across all locations. However, since the dose reproducibility of the dosimeter RaySafe i3 used in the experiment is 10%, it affects the dose ratio error. Furthermore, factors such as the angle dependence of the dosimeter and the spatial resolution of the simulation data contribute to errors in the dose ratio. A previous study evaluated the percent difference in scatter distribution with a five-degree CRA angle at 80 kVp, along with a patient couch displacement of 5 cm to the left of the isocenter measured from a top-down viewpoint, which fell within approximately 20% [23]. Despite these diverse factors, the accuracy of the reproduced scattered radiation distribution within the X-ray room was within approximately 20% of the percent difference as observed in previous studies.

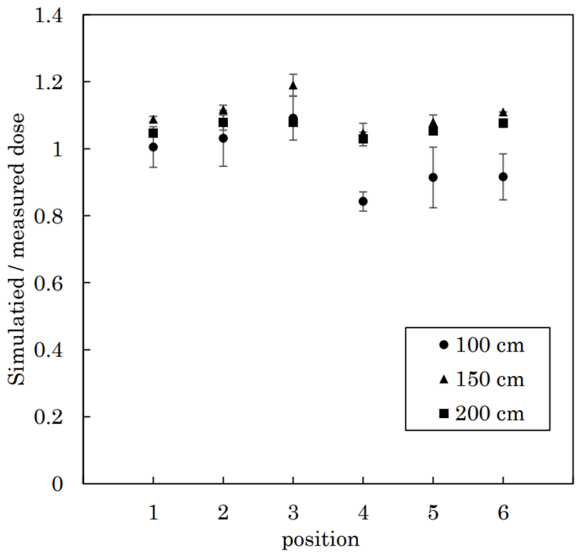

Figure 7. Ratio of simulated and measured values at each position and height in the X-ray room.

3.3. Verification of Position Detection Precision

Figure 8 illustrates the disparity between the distance estimated by our system and the actual measured values for each joint point based on the AR marker. It is evident that the measured values tend to exceed the estimated values as the distance from the camera increases. Furthermore, the error in body tracking is comparatively smaller for the hand than for the eye. This discrepancy arises because the mannequin faces sideways toward the camera, which makes eye-tracking difficult. Notably, measurements at the furthest position from the camera exhibit a considerable standard deviation, which can be attributed to the utilization of the wide field of view (WFOV) unbind mode of Azure Kinect's camera. The WFOV unbind shooting mode allows for high-resolution imaging with a wide field of view. The specified measuring distance of the WFOV unbind mode ranges from 0.25 to 2.88 m. However, at position 1, located farthest from the camera, the distance between the camera and the mannequin is 3.5 m, significantly exceeding the specified measuring distance of WFOV. Consequently, a large standard deviation is observed, which must be considered when operating the system within its designated range.

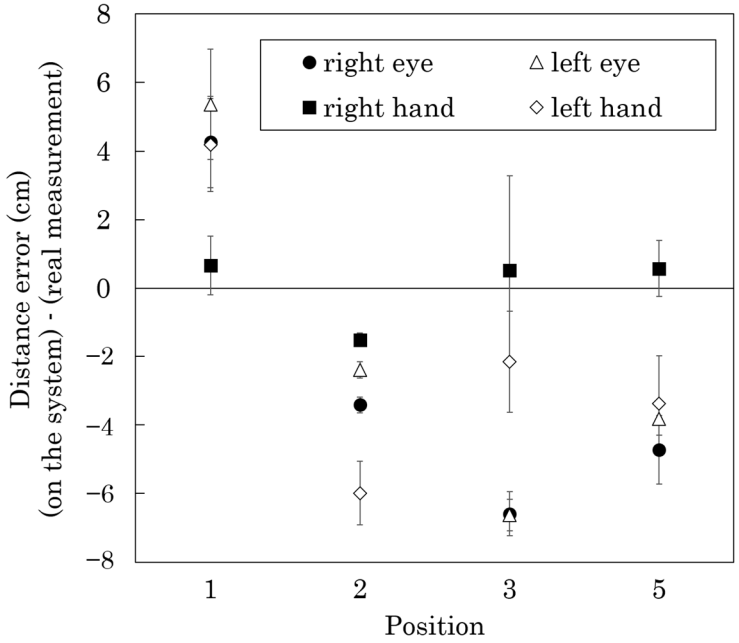

Figure 8. Difference between the distance estimated by the system and the measured value of each joint point from the AR marker.

3.4. Verification of Real-Time Performance

Table 2 presents the results obtained from measuring the average frame rate based on 10 randomly selected values while the system operated under four distinct physician conditions as follows: with and without the physician moving at 25 cm/s and with and without the protective apron. The FPS values recorded were 10.8 without motion and without the protective apron, 11.0 with motion and without the protective apron, 9.0 with motion and with the protective apron, and 9.8 with both motion and the protective apron. Fluoroscopy-guided procedures are performed while wearing protective aprons. Thus, it was essential to ensure that the system maintained real-time performance regardless of apron use. Hence, comparisons were conducted under all four conditions. Subjective observations during system operation did not reveal any issues. Welch's *t*-test was performed at a 5% significance level, aiming to ascertain whether a statistically significant difference in FPS existed among the various physician conditions. Without the apron, there was no statistical advantage in FPS with or without physician motion. With the apron, the FPS decreased significantly. When wearing the apron, the FPS was also significantly reduced for movement.

Table 2. Comparison of the frame rate with and without protective clothing and movement of the physician.

Apron	Motion	Average FPS	
−	−	10.9 ± 0.7	N.S.
−	+	11.0 ± 0.7	S.S.D.
+	−	9.0 ± 0.5	S.S.D.
+	+	9.8 ± 0.4	S.S.D.

S.S.D.: statically significant difference. N.S.: not significant. + indicates that the apron is on and the physician is moving. − indicates that the apron is not on and the physician is not moving.

The verification of real-time performance in terms of FPS aligns with human temporal resolution, typically within the range of 50 ms to 100 ms. Therefore, an output of approximately 10 FPS is deemed acceptable without causing recognition issues. This system meets this expected level, demonstrating smooth operation without discernible problems. Troville et al. [24] indicated that body tracking of the waist, neck, and head remains reliable even when a protective apron is worn. Consequently, within our developed system, body tracking maintained accuracy, and none of the tested conditions significantly affected the system's real-time performance.

3.5. Verification of Dose Estimation Accuracy

Figure 9 shows the results of dose measurements. The vertical axis of the figure displays the personal dose equivalent per mGy of the entrance surface dose. The measured dose represents the personal dose equivalent at the body surface of the mannequin obtained by the dosimeter, whereas the estimated dose indicates the personal dose equivalent at the body-tracked joint points. Table 3 displays the dose ratios between our system's estimations and the measurements taken at evaluation points on the mannequin. The mannequin was oriented toward the couch and positioned horizontally relative to the camera. The dose ratios ranged from 0.60 to 1.21 times for each joint. Notably, the estimated doses were 0.93 to 1.21 times higher than the actual measurements at all joint points except the chest and pelvis. In these two areas, the estimated doses were lower than the measured ones, with estimated values being 0.72 and 0.60 times lower than the measured doses, respectively. This difference can be attributed to the thicker body anatomy of the chest and pelvis compared with the other measured joint points. The system tracked the torso, while actual measurements were taken directly on the body surface. This was because the dosimeters could not be placed inside the mannequin's body. Therefore, the disparity in measurement position significantly influenced the observed dose ratios.

Figure 10 depicts the dose values in the direction of the physician's body thickness from the center of the irradiation field at the height of the physician's chest, considering the scattered radiation distribution used in this system. During the experiment, the mannequin's body surface was approximately 80 cm from the center of the irradiation field, with a body thickness of 20 cm. Under these conditions, the difference between the measured and estimated values from the simulation was about 20%.

Table 3. The dose ratio between the system and each measured evaluation point using the mannequin.

	(Simulated/Measured Dose)		
Position	**1**	**2**	**3**
Right eye	0.94	0.93	0.98
Left eye	1.04	1.01	1.00
Neck	0.98	0.99	0.98
Chest	0.72	0.72	0.78
Pelvis	0.67	0.60	0.94
Right hand	1.19	1.21	1.08
Left hand	1.00	1.19	1.14

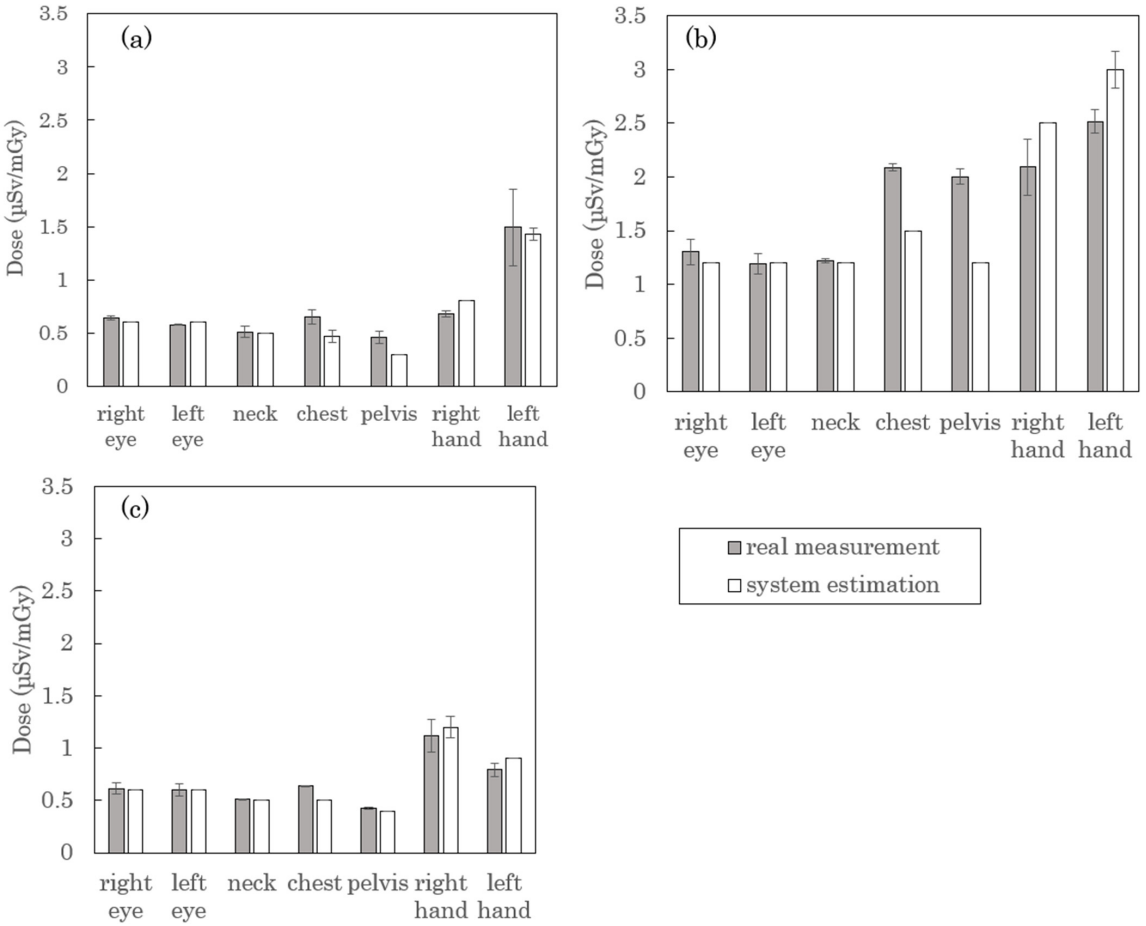

Figure 9. Measured and estimated doses at seven joint points (right eye, left eye, neck, chest, pelvis, right hand, and left hand). (**a**) shows the dose at 1 in Figure 3, (**b**) shows the dose at 2 in Figure 3, and (**c**) shows the dose at 3 in Figure 3. The vertical axis unit is the individual dose equivalent of each site per 1 mGy of the entrance surface dose to the patient.

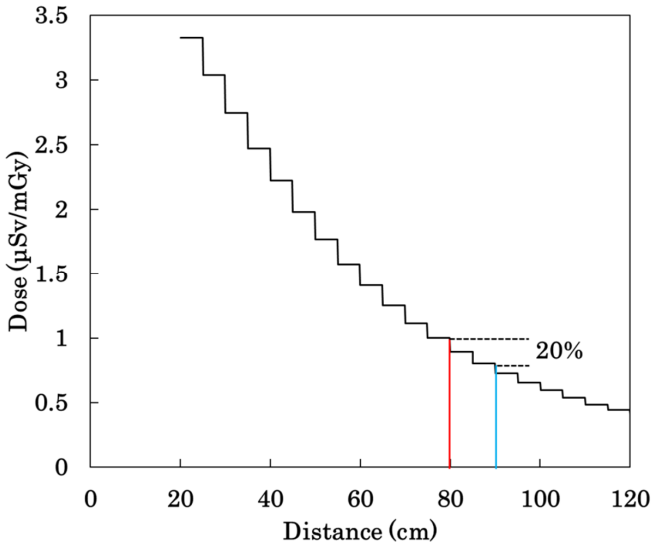

Figure 10. Variation in dose across the thickness at chest height. The red line shows the radiation dose at a position 90 cm away, and the light blue line shows the radiation dose at a position 90 cm away.

4. Discussion

The system developed in this study utilizes body tracking and scattered radiation visualization techniques to provide a real-time multidimensional relationship between scattered radiation and the position of a physician in a virtual reality (VR) environment. Furthermore, by employing AR technology, two-dimensional cross-sections of scattered radiation distribution are displayed in the real-world space, enhancing realism. This system offers a valuable tool for users to understand scattered radiation distribution within an X-ray room intuitively. Additionally, through a collision detection approach, it is possible to estimate the physician's radiation dose in real time regardless of the position of dosimeters (including fingertips and the head). This is useful as an educational tool when staff members need training on radiation doses during fluoroscopic examinations. Without actual exposure, physicians can move within the X-ray room and estimate how their actions correlate with radiation exposure, thus increasing their awareness of personal exposure and the potential to implement appropriate radiation protection measures.

Differences in body surface and distance at body-tracking joint points were found to affect the difference from dosimetry estimation. In order to estimate the dose closer to the dosimeter, a 3D model of the physician's body surface could be created, and the dosimeter installation position could be used as the dose assessment point. Periodic calibration of the dosimeters is also necessary, and the accuracy could be improved by using correction constants to adjust the doses easily.

In recent years, there has been an increasing demand for radiation protection training for staff outside of the radiation and cardiovascular departments among radiation workers [25–28]. It is known that physicians and nurses are particularly exposed to high levels of radiation during fluoroscopic procedures, including IVR and endoscopic retrograde cholangiopancreatography, and education for these professions is important [28,29]. This system matches as an educational tool. Furthermore, some research has shown that even among radiological technologists who have received specialized training in radiation, there are individual differences in awareness [30], so this tool is also effective in educating radiological technologists.

While this research focuses on the specific machine and irradiation condition, simulations involving other machines and varying irradiation conditions can be conducted to estimate radiation doses under different circumstances. In this study, the simulations were performed under standard conditions only. Future work should test the simulations with different tube voltages, irradiation field sizes, focus-to-detector distances, and irradiation angles. Considering the widespread use of protective plates in clinical practice, incorporating simulations with these plates can also assess their shielding effects. Obtaining simulation data allows for understanding the radiation exposure dose and the effectiveness of shielding plates in various conditions, making it valuable for radiation protection education.

Moreover, prior research has used head-mounted displays to acquire radiation doses in VR space. However, this requires individual devices for each person, which is not efficient for educating large groups. In contrast, the system proposed in this study can facilitate education efficiently with just a depth camera and a computer, enabling individuals to take turns entering the X-ray room for training. Additionally, by estimating radiation doses in real space, the proposed system is more realistic and thus more effective for radiation protection education compared with VR-based education.

Currently, the dose estimation function, particularly for the chest and pelvis, is lower than the actual measured doses. This leads to an underestimation of exposure. However, this issue was identified through the accuracy evaluation in this study. To address this in education, individuals can be prompted to adjust the estimated doses by applying factors, ensuring they do not underestimate but rather overestimate their doses.

The findings from this study may allow for future detailed assessment of the unequal exposure of physicians and other medical staff from minimal dosimeters. In particular, fingertips and other areas that may enter the irradiation field are highly exposed and at high

risk of radiation injury. However, there is a problem of difficulty in wearing dosimeters for hygienic and procedural reasons. This method may provide a solution to this problem.

One idea for incorporating this system into an existing training program would be to add a scenario in which the user actually stands in the position where the procedure is to be performed and quantifies the optimal protection and protective effect in terms of dose. The numerical values can be used to determine how much exposure can be reduced by slight differences in the position of the patient during the actual procedure.

In addition, it may be possible to estimate the type of protective equipment and lead equivalent required to optimize protection based on the typical irradiation dose in an examination and the number of examinations performed at a facility.

In addition to the above considerations, future improvement items include marker-less positioning of the device and real-time estimation of dose distribution considering freely moving radiation shielding plates.

5. Conclusions

The developed system, created using body tracking with a depth camera, allowed for the display of arbitrary two-dimensional cross-sections of scattered radiation distribution on a point cloud, thus facilitating real-time dose estimation. The simulated scattered radiation data used for dose estimation showed a 20% error compared with the actual measurement. The FPS parameter of the system was approximately 10, indicating real-time performance. The system successfully estimated doses for multiple joint points from 0.6 to 1.2 times the actual dose, indicating good accuracy. The system proposed in this study, capable of visualizing scattered radiation distribution and estimating physician exposure, has the potential to serve as a new radiation protection education tool.

Author Contributions: Conceptualization, T.F.; methodology, T.F.; software, T.F.; validation, T.F.; formal analysis, T.F.; investigation, T.F. and H.A.; resources, T.F.; data curation, T.F.; writing—original draft preparation, T.F.; writing—review and editing, H.A. and C.A.; visualization, T.F.; supervision, T.F.; project administration, T.F.; funding acquisition, T.F. All authors have read and agreed to the published version of the manuscript.

Funding: This research was funded by JSPS KAKENHI Grant Numbers JP23K24960 and JP21K07703. This study was supported in part by an Industrial Disease Clinical Research Grant (220201-01) from Japan.

Institutional Review Board Statement: Not applicable.

Informed Consent Statement: Not applicable.

Data Availability Statement: The datasets presented in this article are not readily available because the data are part of an ongoing study. Requests to access the datasets should be directed to the corresponding author.

Acknowledgments: We would like to thank Kenta Honiden, Department of Health Sciences, Kyushu University Graduate School of Medicine, for his cooperation in data acquisition during this study.

Conflicts of Interest: The authors declare no conflicts of interest.

References

1. Kim, K.P.; Miller, D.L. Minimising radiation exposure to physicians performing fluoroscopically guided cardiac catheterisation procedures: A review. *Radiat. Prot. Dosim.* **2009**, *133*, 227–233. [CrossRef] [PubMed]
2. Hizukuri, K.; Fujibuchi, T.; Arakawa, H. Directional Vector Visualization of Scattered Rays in Mobile C-arm Fluoroscopy. *Radiol. Phys. Technol.* **2024**, *17*, 288–296. [CrossRef]
3. International Commission on Radiological Protection (ICRP). *Avoidance of Radiation Injuries from Medical Interventional Procedures*; ICRP Publication 85; Pergamon: Oxford, UK, 2000; Volume 30.

4. Dauer, L.T.; Thornton, R.H.; Solomon, S.B.; St Germain, J. Unprotected operator eye lens doses in oncologic interventional radiology are clinically significant: Estimation from patient kerma-area-product data. *J. Vasc. Interv. Radiol.* **2010**, *21*, 1859–1861. [CrossRef] [PubMed]
5. Vano, E.; Gonzalez, L.; Fernandez, J.M.; Haskal, Z.J. Eye lens exposure to radiation in interventional suites: Caution is warranted. *Radiology* **2008**, *248*, 945–953. [CrossRef] [PubMed]
6. IAEA. *Implications for Occupational Radiation Protection of the New Dose Limit for the Lens of the Eye*; IAEA: Vienna, Austria, 2013; Volume 1731, pp. 1–34.
7. Chida, T. What are useful methods to reduce occupational radiation exposure among radiological medical workers, especially for interventional radiology personnel? *Radiol. Phys. Technol.* **2022**, *15*, 101–115. [CrossRef]
8. Chida, K.; Takahashi, B.T.; Ito, D.; Shimura, H.; Takeda, K.; Zuguchi, M. Clarifying and visualizing sources of staff-received scattered radiation in interventional procedures. *AJR Am. J. Roentgenol.* **2011**, *197*, W900–W903. [CrossRef]
9. Haga, Y.; Chida, K.; Kaga, Y.; Sota, M.; Meguro, T.; Zuguchi, M. Occupational eye dose in interventional cardiology procedures. *Sci. Rep.* **2017**, *7*, 569. [CrossRef]
10. Rodas, N.L.; Barrera, F.; Padoy, N. See It with your own eyes: Markerless mobile augmented reality for radiation awareness in the hybrid room. *IEEE Trans. Biomed. Eng.* **2017**, *64*, 429–440. [CrossRef]
11. Nishi, K.; Fujibuchi, T.; Yoshinaga, T. Development and evaluation of the effectiveness of educational material for radiological protection that uses augmented reality and virtual reality to visualise the behaviour of scattered radiation. *J. Radiol. Prot.* **2022**, *42*, 011506. [CrossRef]
12. Fujibuchi, T. Radiation protection education using virtual reality by visualization of scatter distribution in radiological examination. *J. Radiol. Prot.* **2021**, *41*, S317. [CrossRef]
13. Fujibuchi, T.; Ueda, K.; Kadoyanagi, S.; Ueno, D.; Nakamura, C. Examination of application to radiation protection education by four-dimensional visualization of scatter distribution in radiological examination using virtual reality. *Nihon Hoshasen Gijutsu Gakkai Zasshi* **2019**, *75*, 1297–1307. [CrossRef] [PubMed]
14. Süncksen, M.; Bott, O.J.; Dresing, K.; Teistler, M. Simulation of scattered radiation during intraoperative imaging in a virtual reality learning environment. *Int. J. Comput. Assist. Radiol. Surg.* **2020**, *15*, 691–702. [CrossRef] [PubMed]
15. Takata, T.; Kondo, H.; Yamamoto, M.; Shiraishi, K.; Kobayashi, T.; Furui, S.; Okamoto, T.; Oba, H.; Kotoku, J. Immersive Radiation Experience for Interventional Radiology with Virtual Reality Radiation Dose Visualization Using Fast Monte Carlo Dose Estimation. *Interv. Radiol.* **2020**, *5*, 58–66. [CrossRef] [PubMed]
16. Sato, T.; Iwamoto, Y.; Hashimoto, S.; Ogawa, T.; Furuta, T.; Abe, S.I.; Kai, T.; Tsai, P.E.; Matsuda, N.; Iwase, H.; et al. Features of Particle and Heavy Ion Transport code System (PHITS). version 3.02. *J. Nucl. Sci. Technol.* **2018**, *55*, 684–690. [CrossRef]
17. Hirayama, H.; Namito, Y.; Bielajew, A.F.; Wilderman, S.J.; Nelson, W.R. The EGS5 code system SLAC-R-730 and KEK Report 2005–8. Stanford (California) and Tsukuba: SLAC and KEK; 2005. *J. Nucl. Sci. Technol.* **2018**, *55*, 684–690. [CrossRef]
18. PHOTX. *Photon Interaction Cross-Section Library for 100 Elements Data Package DLC136/PHOTX*; Radiation Shielding Information Center Oak Ridge National Laboratory: Oak Ridge, TN, USA, 1995. Available online: https://www.oecd-nea.org/tools/abstract/detail/dlc-0136/ (accessed on 10 September 2024).
19. Kato, H.; Fujii, S.; Shirakawa, S.; Suzuki, Y.; Nishii, Y. A Presumption Calculating Formula of the X-ray Spectrum Generated from a Molybdenum Target X-ray Tube. *Jpn. J. Radiol. Technol.* **2011**, *67*, 193–201. [CrossRef] [PubMed]
20. ICRP Publication 74. Conversion coefficients for use in radiological protection against external radiation. *Ann. ICRP* **2016**, *26*, 3–4.
21. GitHub Microsoft/Azure-Kinect-Samples. Available online: https://github.com/microsoft/Azure-Kinect-Samples (accessed on 19 May 2022).
22. Hattori, K.; Inaba, Y.; Kato, T.; Fujisawa, M.; Yasuno, H.; Yamada, A.; Haga, Y.; Suzuki, M.; Zuguchi, M.; Chida, K. Evaluation of a New Real-Time Dosimeter Sensor for Interventional Radiology Staff. *Sensors* **2023**, *23*, 512. [CrossRef]
23. Troville, J.; Rudin, S.; Bednarek, D.R. Estimating Compton scatter distributions with a regressional neural network for use in a real-time staff dose management system for fluoroscopic procedures. *Proc. SPIE Int. Soc. Opt. Eng.* **2021**, *11595*, 115950M. [CrossRef]
24. Troville, J.; Dhonde, R.S.; Rudin, S.; Bednarek, D.R. Using a convolutional neural network for human recognition in a staff dose management software for fluoroscopic interventional procedures. *Proc. SPIE Int. Soc. Opt. Eng.* **2021**, *11595*, 115954E. [CrossRef]
25. Rehani, M.M.; Ciraj-Bjelac, O.; Vañó, E.; Miller, D.L.; Walsh, S.; Giordano, B.D.; Persliden, J. *Radiological Protection in Fluoroscopically Guided Procedures Outside the Imaging Department*; Elsevier: Amsterdam, The Netherlands, 2010; Volume 40, pp. 1–102. [CrossRef]
26. ICRP. Occupational radiological protection in interventional procedures. ICRP Publication 139. *Ann. ICRP* **2018**, *47*, 1–118. [CrossRef] [PubMed]
27. ICRP. Education and Training in Radiological Protection for Diagnostic and Interventional Procedures; ICRP Publication 113. *Ann. ICRP* **2009**, *39*, 1–68. [CrossRef]
28. Matsuzaki, S.; Moritake, T.; Morota, K.; Nagamoto, K.; Nakagami, K.; Kuriyama, T.; Kunugita, N. Development and assessment of an educational application for the proper use of ceiling-suspended radiation shielding screens in angiography rooms using augmented reality technology. *Eur. J. Radiol.* **2021**, *143*, 109925. [CrossRef] [PubMed]

29. Chida, K.; Kaga, Y.; Haga, Y.; Kataoka, N.; Kumasaka, E.; Meguro, T.; Zuguchi, M. Occupational dose in interventional radiology procedures. *Am. J. Roentgenol.* **2013**, *200*, 138–141. [CrossRef]
30. Yashima, S.; Chida, K. Awareness of Medical Radiologic Technologists of Ionizing Radiation and Radiation Protection. *Int. J. Environ. Res. Public Health* **2022**, *20*, 497. [CrossRef]